Title
Investigation of a continuous crystal PSAPD-based gamma camera

Journal
IEEE Transactions on Nuclear Science, 53(3)

ISSN
0018-9499

Authors
Després, P
Barber, W C
Funk, T
et al.

Publication Date
2006-06-01

Peer reviewed

Investigation of a Continuous Crystal PSAPD-based Gamma Camera

Philippe Després*, William C. Barber, Tobias Funk, Mickel McClish, Kanai S. Shah and Bruce H. Hasegawa

***Abstract*— Position-sensitive avalanche photodiodes (PSAPDs) have recently been proposed as optical light detectors in scintillation based gamma cameras. They are compact solid-state devices that provide high quantum efficiency and gain, and they can achieve precise positioning over relatively large surfaces with few readout channels. In previous studies, PSAPDs were coupled to scintillator arrays and the imaging task consisted in identifying the crystal of interaction. In this work, we investigate the possibility of using a PSAPD to read the light of a single continuous crystal. Such a configuration has the potential to reduce the cost and simplify the construction of a PSAPD-based gamma camera while maintaining good overall performance. The spatial resolution of a small imaging unit having a continuous scintillator coupled to an 8x8 mm^2 PSAPD was evaluated at different energies for CsI:Tl and $LaBr_3$:Ce crystals. After correcting the images for the distortion and the minification associated with this camera, spatial resolution values of 0.62, 0.72, 0.99, and 1.25 mm (FWHM) were obtained for ^{99m}Tc (140 keV), ^{57}Co (122 keV), ^{241}Am (60 keV), and ^{125}I (30 keV) respectively for an 8×8×1 mm^3 CsI:Tl crystal. Corresponding values of 0.55, 0.64, 0.92 and 1.10 mm (FWHM) were obtained from a 1 mm thick $LaBr_3$:Ce crystal. These results, reproduced by Monte Carlo simulations, suggest that the continuous crystal configuration is an attractive approach to develop a PSAPD-based high-resolution gamma camera and is especially well suited for a small-animal imaging system.**

I. Introduction

PSAPDs are an attractive alternative to photomultiplier tubes (PMTs) as photodetectors in the design of gamma-ray detectors for medical imaging. As with other solid-state devices, they offer compactness, high quantum efficiency and high gain. PSAPDs have also shown good spatial resolution over relatively large surfaces with few readout channels [1], a key feature that constitutes an economical advantage over other solid-state solutions, like CZT, which require a readout channel for each pixel. A large area detector with a reduced number of readout channels is especially appealing for the development of a low-cost, high-performance solid-state imaging system. For example, an 8x8 mm^2 PSAPD can be used to read an 8x8 crystal array of the same size, but with 16 times fewer channels than a pixelated system would require. This feature allows us to envision a solid-state system at a comparable or lower cost than actual solutions based on PMTs.

Manuscript received April 4, 2006. This work was supported in part by the National Institutes of Health under Grant No. 2R44 HL078295-02.

P. Després, W. C. Barber, T. Funk and B. H. Hasegawa are with the Physics Research Laboratory, University of California, San Francisco, 185 Berry St. Suite 350, San Francisco, California 94107

M. McClish and K. S. Shah are with Radiation Monitoring Devices Inc., 44 Hunt St., Watertown, Massachusetts 02472

*Corresponding author. email: pdespres@radiology.ucsf.edu

Most imaging studies conducted with PSAPDs have been performed with arrays of small crystals, for both SPECT and PET applications [1]–[5]. However, the analog nature of the charge division in PSAPDs theoretically could be utilized to derive the position of an event in a continuous crystal, with a minimal loss in spatial resolution. Such a configuration is particularly attractive for SPECT, where a single continuous crystal offers cost and simplicity advantages in comparison to designs that use a segmented scintillator. The continuous crystal approach was explored in this work with a simple camera having a single crystal coupled to a PSAPD. In parallel, Monte Carlo simulations of this setup were conducted with the goal of reproducing the experimental results. The validation of the simulations will allow us to use them to predict the behavior of larger systems made of multiple PSAPDs.

II. Materials and methods

A. Experiment

An 8x8 mm^2 PSAPD from Radiation Monitoring Devices (RMD Inc., Watertown MA) was used in this work. The PSAPD is packaged on a ceramic substrate with five pins (four corner anodes and one cathode) connected individually to a readout circuit board where five Cremat CR-110 charge sensitive preamplifiers (Cremat, Inc. Watertown, MA) are used to collect the signals. The preamplified signals are then fed in Canberra 2020 amplifiers (Canberra Industries, Meriden, CT) having shaping times of 250 ns. The signal from the cathode was used to trigger a sample-and-hold board that fed the shaped signals to a Keithley DAS-1801HC acquisition board on a personal computer, where events were recorded in list mode. A noise problem with the sample-and-hold board prevented the use of longer shaping times, which would have been beneficial in the case of the CsI:Tl crystal, given its long decay time (see Table I). This problem, combined with temperature drift and small gain variations over the PSAPD surface, made reliable spectroscopic measurements difficult to obtain. Also, no energy window was used to create the images for ^{125}I and ^{241}Am, while a large window of [≈-40%,∞] around the main photopeak was used for ^{57}Co and ^{99m}Tc.

The positions of the interactions were computed using Anger logic from the signals (S_i) of the four corners ($i = 1, 2, 3, 4$):

$$x_{Anger} = \frac{(S_2 + S_3) - (S_1 + S_4)}{(S_1 + S_2 + S_3 + S_4)}$$
$$y_{Anger} = \frac{(S_1 + S_2) - (S_3 + S_4)}{(S_1 + S_2 + S_3 + S_4)}. \quad (1)$$

The event positions obtained with Eq. 1 were rebinned into 200×200 two-dimensional histograms to create images, corresponding to a pixel size of 40×40 μm^2.

The PSAPD was optically coupled to a continuous 8x8x1 mm^3 CsI:Tl crystal (Hilger Crystals, UK) encapsulated in white epoxy resin. A continuous $LaBr_3$:Ce crystal from RMD Inc. was also used. This crystal had a cylindrical shape with a diameter of 7 mm, a thickness of approximately 1 mm and slightly rounded edges. It was enclosed in epoxy and aluminum except for a 0.25 mm transparent light output window.

The PSAPD, the crystal and the readout board with the preamplifiers were placed in a light-tight aluminum enclosure, as shown in Fig. 1. A continuous flow of cooled dry nitrogen gas in the enclosure, together with a cold support plate, kept the temperature of these devices at -60±1°C, to minimize the dark current in the PSAPD. The PSAPD was operated at a bias voltage of -1600 V, for a gain of approximately 1000.

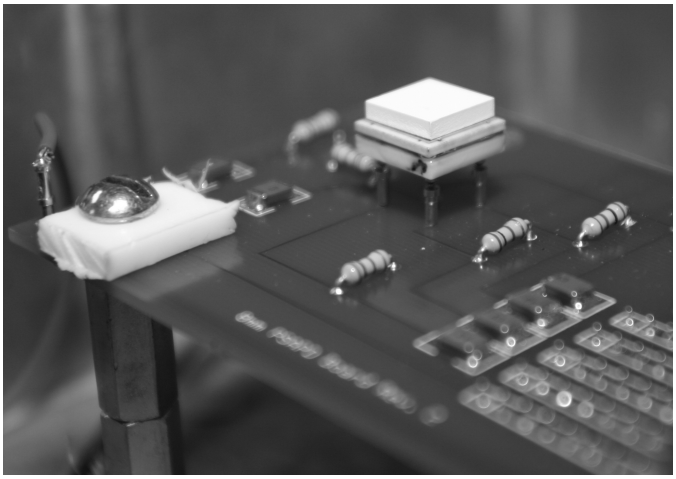

Fig. 1. The white epoxy covered CsI:Tl crystal sitting on the PSAPD. The preamplifiers are located under the PC board.

B. Spatial resolution

The spatial resolution of this simple system was measured for ^{99m}Tc (140 keV), ^{57}Co (122 keV), ^{241}Am (60 keV), and ^{125}I (30 keV). Point spread functions (PSFs) were acquired by irradiating the crystal with a pencil beam near its center. The pencil beam was created by positioning the sources one meter from a 0.5 mm diameter lead pinhole located 15 mm over the crystal surface. The effective diameter of the pinhole [6], taking into account penetration through its edges, was 0.51, 0.515 and 0.52 mm for ^{241}Am, ^{57}Co and ^{99m}Tc respectively. For ^{125}I, a 0.1 mm pinhole in a lead sheet was placed directly over the crystal, and edge penetration was negligible. This allowed us to position the weaker ^{125}I source closer to the detector without creating a divergent beam in the crystal. The lead sheet pinhole was not used with the other sources because of penetration and scatter problems. The raw spatial resolutions were calculated as the full-width at half-maximum (FWHM) of a Gaussian fit through a profile in the resulting image. These raw measurements were then corrected to account for three effects affecting the spatial metric of the system: a DC offset in the ADC channel values, a pincushion distortion caused by the Anger-logic linear readout of a nonlinear charge dispersion in the resistive layer, and a minification effect caused by the single crystal configuration. Section II-D below describes these effects and how the spatial resolution was corrected to account for them.

C. Imaging

Two simple imaging experiments were conducted with a 0.5 mm lead pinhole to evaluate the ability of the continuous crystal camera to produce images. In a first experiment, images of brachytherapy seeds were acquired in a unit magnification setup, as shown in Fig. 2. The seeds contain two ^{125}I beads (≈30 keV) each having a 0.5 mm diameter, located 3.6 mm apart and encapsulated in a titanium casing. The two seeds were positioned approximately 3.5 mm apart and imaged side-by-side and parallel to each other, so that the four radioactive beads formed a square in the image. In the second experiment, three capillary tubes filled with ^{99m}Tc were imaged, again with unit magnification. The capillary tubes had an internal diameter of 0.58 mm and an external diameter of 1 mm. The three radioactive tubes were separated by two empty ones, so that the total distance between two line sources was 3 mm.

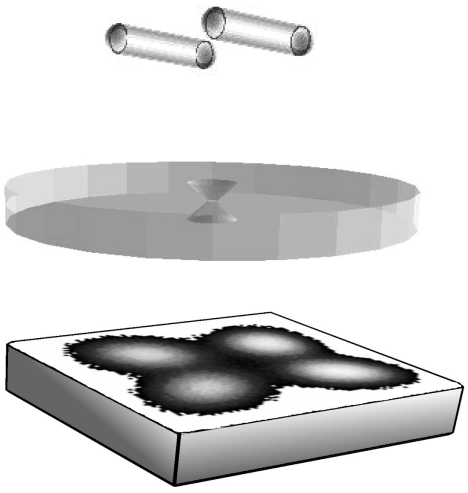

Fig. 2. A schematic representation of the brachyseed imaging experiment. Two seeds side-by-side were imaged through a 0.5 mm pinhole located at mid-distance (15 mm) between the sources and the scintillation crystal. A similar experiment was conducted with three capillary tubes filled with ^{99m}Tc. The pinhole was also used to create pencil beams in the crystal, in which case the sources were located one meter from the pinhole.

D. Simulations

A noise model of the detection chain was developed to assess the ability of a single PSAPD to perform event positioning. The noise behavior of a PSAPD is, in most respects, identical to that of a normal avalanche photodiode, as described in several publications (*e.g.* [7] and references therein). Additional considerations arise from the charge division in the

resistive layer. In this work, it is assumed that the total charge is preserved but is divided between four independent channels according to a sharing map that reproduces the observed distortion pattern [8].

For an APD, the variance in the signal is given by

$$\sigma_N^2 = M^2\sigma_{N_0}^2 + M^2 N_0(F-1) + \sigma_\delta^2. \quad (2)$$

where M is the gain, N_0 is the initial number of charges, F is the excess noise factor and σ_δ is the APD-preamplifier noise. Experimental estimations of F suggested that it increases linearly with the gain and that it is approximately independent of temperature [9]–[11]. For instance, Solovov *et al.* [9] found that $F = k_F M + F_0$ with $k_F = 0.00239 \pm 0.00008$ and F_0=1.87±0.02 for $M > 100$.

Considering the correlations between the signals from the four channels of a PSAPD, the distribution of the optical light on its surface and the nonlinear charge division, an analytical expression for the spatial positioning error cannot be easily derived from Eq. 2. Instead, a Monte Carlo framework was developed to reproduce the positioning performance of the PSAPD. Although the GATE package [12] is designed specifically for nuclear medicine system modeling, a native GEANT4 (version 4.8) [13] application was developed to allow a better control of the simulation. Moreover, GATE does not yet allow the simulation of optical photons, an important part of the present work. The GEANT4 library contains an implementation of the DETECT transport and boundary models developed initially by Knoll *et al.* [14] and then by Levin and Moisan [15].

The GEANT4 application, reproducing the geometry of the experimental setup, was run to record the spatial distribution of the detected optical light on the PSAPD surface. The scintillation photons were generated as a pure Poisson process, *i.e.*, that the intrinsic resolution of the crystal was not considered. The simulated crystal was wrapped in a material acting as a Lambertian or diffuse reflector [16] having a reflection coefficient of 0.98. The interface was modeled as paint over a ground finish, and the boundary processes followed the rules of the unified model developed for the DETECT project [15]. As in the experimental setup, the simulated crystal was coupled to the PSAPD with a thin layer (50 μm) of optical grease having a refraction index of 1.46. The grease thickness was set to 300 μm for the $LaBr_3$ simulations to account for the presence of the 0.25 mm window on this crystal. The PSAPD surface was modeled as a polished quartz window, assuming an experimentally derived value for quantum efficiency [17]. The optical properties of the materials involved in the simulations – refraction index, scintillation wavelengths and absorption lengths – were gathered from various sources [18], [19]. These data were implemented as a function of the wavelength in the simulations, when this information was available. Table I reports the optical constants used for the simulations, along with other material characteristics.

The spatial light distribution produced by each event was recorded in two-dimensional histograms and stored as a tree structure in a ROOT (version 5.08) [20] file for further processing. Figure 3 shows a typical distribution of detected light on the PSAPD surface resulting from a single scintillation event in a square continuous crystal coupled to the photodiode.

TABLE I
SUMMARY OF MATERIAL PROPERTIES

Property	CsI:Tl	$LaBr_3$:Ce	PSAPD
Density (g/cm^3)	4.51	5.29	2.33
Light yield (photons/MeV)	55000	75000	NA
Primary decay time (ns)	1000	26	NA
Wavelength @ max emission λ_{max} (nm)	550	380	NA
Refraction index @ λ_{max}	1.78	1.9	1.46 (quartz)
Absorption length @ λ_{max} (cm)	400	400	0.00015
Quantum eff. of PSAPD @ λ_{max}	0.58	0.5	NA

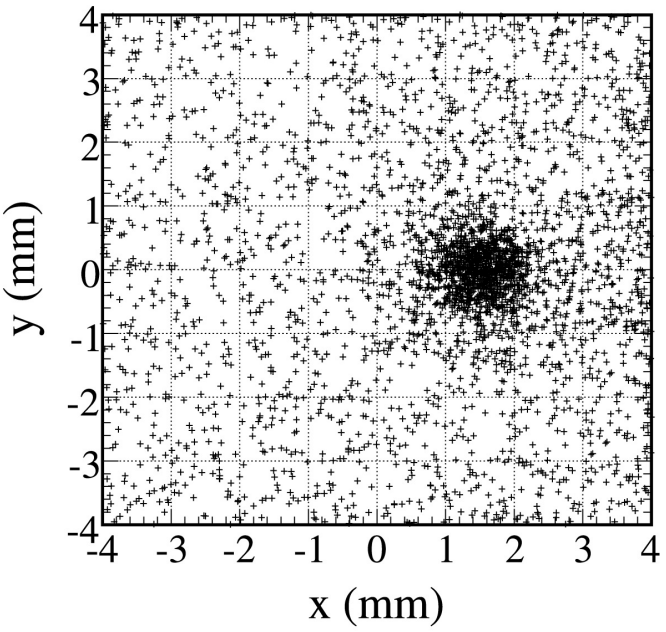

Fig. 3. A typical simulation of detected light distribution on the PSAPD surface following a scintillation event in a continuous crystal. For this particular event, an incoming 140.5 keV gamma ray interacts near mid-depth of an 8x8x1 mm^3 thick CsI:Tl crystal at position 0,1.5 mm, and creates 6149 optical photons, 3473 of which are detected. The stray photons contribute to pull the centroid of the distribution towards the center.

A simple Monte Carlo simulation was conducted to assess the basic imaging properties of the continuous crystal setup. A pencil beam of radiation having an infinitesimal width was scanned across the crystal's central axis and the centroid of the detected light distribution was recorded along with the real beam position. As evident in Fig. 3, the continuous crystal allows optical photons to be detected everywhere on the PSAPD surface. As a consequence of these stray photons, the computed positions are pulled toward the center of the device, and the continuous crystal indeed creates a minification of the object being imaged. The scanned pencil beam simulation was used to estimate this minification value, in order to correct the spatial resolution obtained experimentally.

The pincushion distortion intrinsic to four corner PSAPDs

also pulls computed positions closer to the center. This phenomenon is attributable to the linear Anger-logic scheme used to read a nonlinear charge dispersion in the PSAPD's resistive layer, and contributes to further reduce the size of an object in the image. A finite-element model of the resistive layer [8] was used to estimate the minification for the central region of the device. This method was used successfully to reproduce and correct the pincushion pattern observed in images obtained with a PSAPD and a segmented CsI:Tl scintillator [8]. Figure 4 shows the good agreement of this model with experimental data. In this case, the positions of direct interactions of ^{57}Co in the silicon were recorded. Also apparent in Fig. 4 is the effect of the DC offset in the recorded ADC channel values, which causes the pincushion pattern to shrink. To correct for this effect, a DC value was subtracted from all four channels so that the pattern of direct interactions reaches the corners of the image. This value was subtracted when creating the images used for the resolution measurements.

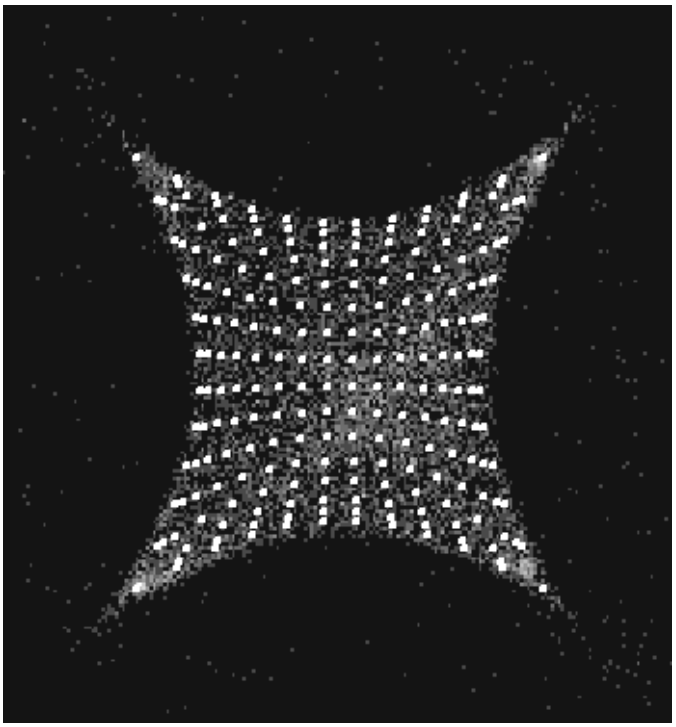

Fig. 4. Positions of direct interactions of ^{57}Co photons in the PSAPD, as computed by Anger-logic. The pincushion pattern is well reproduced by the finite-element model of the resistive layer (white dots). The image is not corrected for the DC offset in the ADC values and therefore the pattern is not stretched out to the corners of the image.

To simulate the signal on each of the four PSAPD channels, the detected charge distribution was multiplied by the gain and then divided according to a sharing map obtained from a finite-element model of the PSAPD's resistive layer. A random quantity, characterized by the values of F and σ_δ, was then added to each channel to account for the multiplication and the preamplifier noise. A measured dark current of 40 nA and the estimated photodiode input capacitance of 12 pF set the noise level to $\sigma_\delta \approx 500$ according to the preamplifier manufacturer. A gain of 1000 and the corresponding value of $F = 4.25$ was assumed, following the results of Solovov *et al.* [9]. Simulated images were created by Anger-logic (Eq. 1) from the simulated channel outputs and were processed to extract the spatial resolution in the same way as the experimental images.

III. Results

Figure 5 shows the results comparing the known and calculated positions from the simulation where a pencil beam of radiation was swept across the crystal's central axis. The center of mass of the detected light distribution is a linear function of the true position of the beam for most of the crystal length. Near the edges, where many optical photons are reflected towards the center of the PSAPD by the crystal's sidewalls, this linear behavior vanishes and degeneracy in positions occurs. This phenomenon limits the imaging capability near the perimeter. For the linear portion of the curve, an energy-independent slope of 0.64 was found for the square CsI:Tl crystal. A corresponding value of 0.54 was found for the 7 mm diameter $LaBr_3$:Ce.

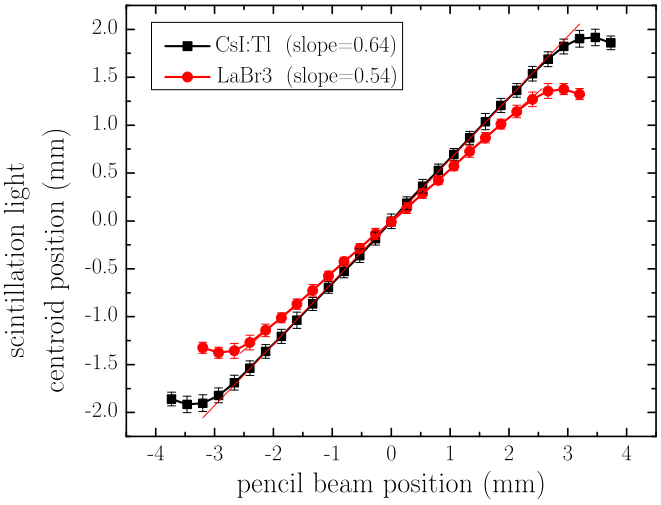

Fig. 5. The center of mass of the detected light distribution on the PSAPD surface as a function of the real position of the event, as obtained by a Monte Carlo simulation, for the CsI:Tl and $LaBr_3$:Ce crystals. These results are used to correct the measured spatial resolutions for the single crystal minification effect.

Figure 6 shows the effect of the pincushion distortion (Fig. 4) on the positions. The associated minification factor, independent of the energy and of the crystal used, is 0.80. Therefore, total minification factors of 1.95 and 2.3 were assumed near the center of the system for the CsI:Tl and $LaBr_3$:Ce crystals respectively. The spatial resolutions obtained experimentally, already corrected for the DC offset in ADC values, were multiplied by these factors in order to give them physical units of length.

A. Spatial resolution

Figure 7 shows a raw PSF profile obtained with the $LaBr_3$:Ce crystal and a pencil beam of ^{125}I. The other PSF profiles are not shown; their FWHM values are rather reported in

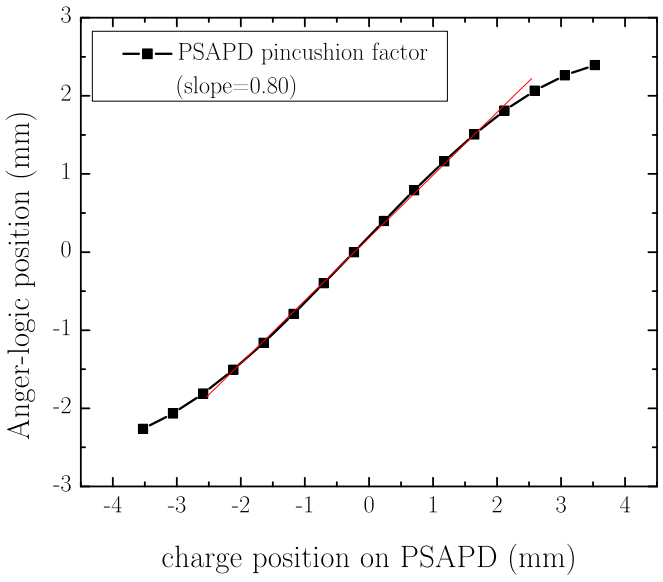

Fig. 6. The minification along the PSAPD central axes caused by the pincushion distortion, as computed by a finite-element model of the resistive layer [8]. The linear portion of the curve has a slope of 0.80.

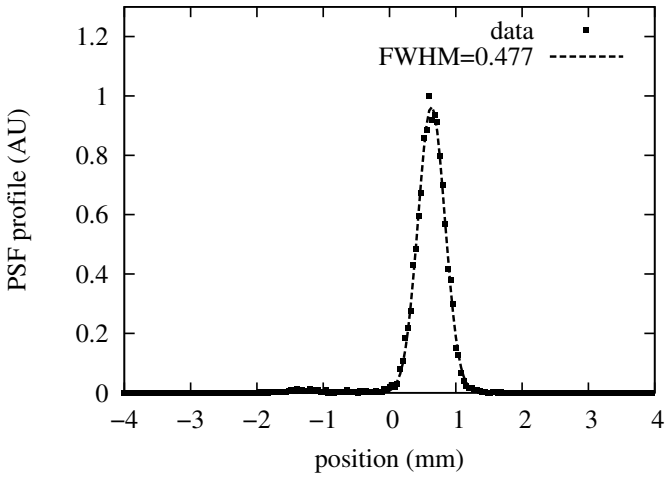

Fig. 7. A point spread function obtained with the $LaBr_3$:Ce crystal and a ^{125}I pencil beam near the crystal center, corrected for DC offset in ADC values. The spatial resolution corrected for pincushion distortion and single crystal minification (combined factor of 2.3) is reported in Table II.

Table II, after correction for the pincushion distortion, the DC offset and the continuous crystal minification. The improved spatial resolution performance of the $LaBr_3$:Ce crystal is due to its higher light yield in comparison to that from CsI:Tl.

TABLE II
SUMMARY OF SPATIAL RESOLUTION RESULTS

Source	main γ (keV)	QE* in 1 mm CsI(%)	QE* in 1 mm $LaBr_3$(%)	CsI:Tl (mm FWHM)	$LaBr_3$:Ce (mm FWHM)
^{125}I	30	97.5	99.9	1.25	1.10
^{241}Am	60	96.7	91.3	0.99	0.92
^{57}Co	122	37.2	27.8	0.72	0.64
^{99m}Tc	140	26.7	19.5	0.62	0.55

* Quantum efficiencies (QE) computed with the photoelectric cross sections from the XCOM database [21].

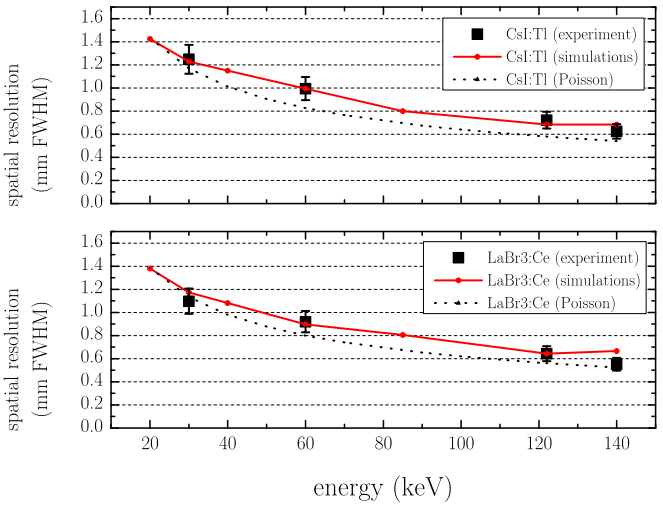

Fig. 8. Simulated and experimental spatial resolutions for different gamma-ray emitters. The values are corrected for DC offset in ADC values, pincushion distortion and continuous crystal minification. An error of 10% was assumed on the experimental data.

Figure 8 compares the experimental spatial resolutions with those obtained from the simulations. An error of 10% was assumed on the experimental data. Also shown is the behavior that one would expect if the spatial resolution followed a $1/\sqrt{N}$ Poisson process. This curve was scaled to match the simulated resolutions at the lowest energy. The modeled and experimental data are in good agreement over the range of energies studied, and follow relatively well the Poisson behavior. A close conformance to the Poisson behavior is not expected however, considering that Compton events and possible fluorescence x-rays following photoelectric events are likely to produce light at locations away from the first interaction and therefore affect the spatial resolution. Nevertheless, the relatively good agreement between experimental and simulated data suggests that the simulation framework developed here can be used to predict the behavior of a larger system made of multiple PSAPDs.

Figures 9 and 10 show the results of the imaging experiments conducted with the continuous crystals. The images obtained were not corrected for pincushion distortion or minification. The beads in Fig. 9 are slightly elongated towards the corners as a result of the pincushion distortion. The two radioactive beads of each seed are clearly resolved. The higher spatial resolution provided by the $LaBr_3$ crystal is also apparent in Fig. 9.

Figure 10 shows the ^{99m}Tc capillary tubes imaged with the $LaBr_3$:Ce crystal. The lines are relatively straight in this case because the light reflection properties within the cylindrical crystal compensate for the pincushion distortion inherent to the PSAPD. The wrapping of positions near the edges, predicted by the simulations (Fig. 5), is responsible for the pile-up of events at both ends of the capillary tubes, and rendered as artificial hot spots in Fig. 10. A line profile was taken near

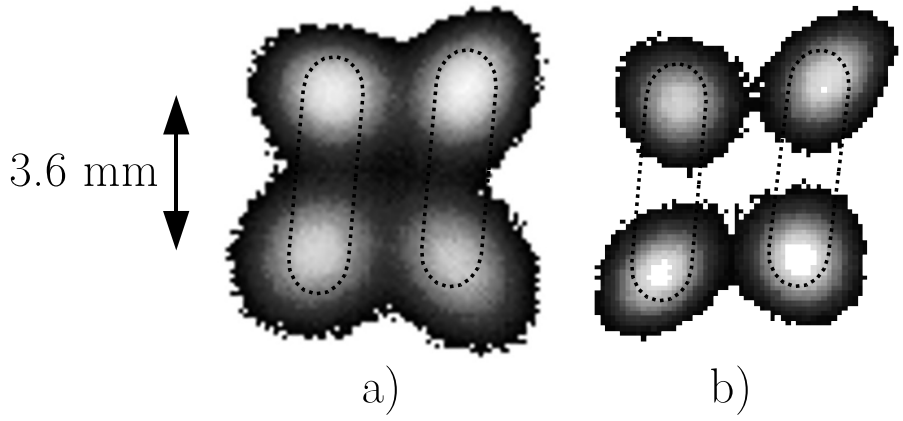

Fig. 9. The ^{125}I brachytherapy seeds imaged with the a) CsI:Tl and b) $LaBr_3$:Ce crystals in a unit magnification setup. The dashed lines show an approximate contour of the seeds in the image. The physical distance between the radioactive beads inside each seed is 3.6 mm.

the center of the capillary tube image, and a peak-to-valley ratio of ≈ 10 was found, as shown in Fig. 11.

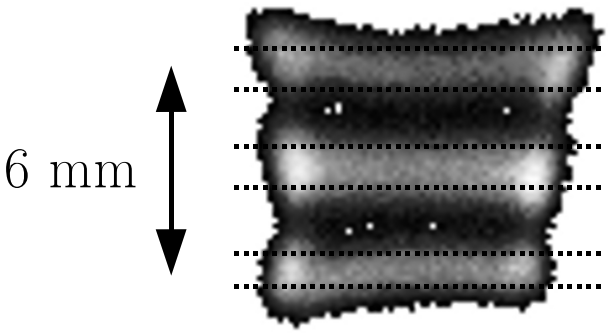

Fig. 10. ^{99m}Tc-filled capillary tubes imaged with the $LaBr_3$:Ce crystal. The hot spots at both ends are due to the position degeneracy that occurs near the crystal's perimeter (see Fig. 5). The dashed lines show the approximate position of the inner diameter of the capillary tubes. The center-to-center physical distance between each tube is 3 mm.

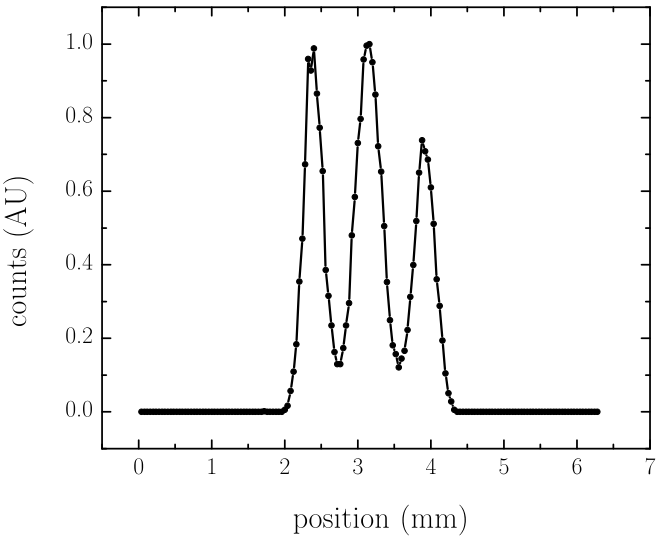

Fig. 11. Profile through the capillary tubes image (Fig. 10).

IV. Discussion

The experiments and simulations conducted with a continuous crystal, PSAPD-based gamma camera suggest that this configuration can be used to obtain high-resolution images of radionuclide distributions. Intrinsic spatial resolutions below or near the millimeter level are reported for energies down to 30 keV. Although the measurements were performed near the center of the device, images of capillary tubes and brachytherapy seeds suggest that good spatial resolution is also preserved away from the center of the device. This demonstration has limitations however, as the area covered by a single PSAPD is too small to be of any practical use. Moreover, the effective imaging area is further limited by the edge effect that introduces positioning errors for locations along the perimeter. For events occurring near the edges, the centroid of the light distribution is pulled toward the center by the stray photons, like for any off-center event, but also by a higher proportion of photons reflected by the crystal's sidewalls. These additional stray photons are responsible for the wrapping or degeneracy of positions near the edges, as seen both in simulations (Fig. 5) and in experiments (pile-up of events near the edges in Fig. 10).

The one-to-one coupling of an encapsulated crystal to a single PSAPD in any case would be a poor approach in implementing an imaging system having multiple PSAPDs. An arrangement in which a single sheet of crystal covers multiple tiled PSAPDs is likely more promising. Moreover, the edge effects in such a configuration would be confined to a much smaller fraction of the total detection area.

The thicknesses of the crystals used for the experiments, 1 mm, is also a factor to consider in the interpretation of

the results. This amount of CsI absorbs about 30% of the 140 keV photons emitted by ^{99m}Tc, a value too low for biomedical applications. $LaBr_3$ is slightly less efficient than CsI for converting 140 keV photons. Increasing the thickness to 4 mm would allow a quantum efficiency of $\approx 75\%$ for CsI and of $\approx 65\%$ for $LaBr_3$ at 140 keV, but is likely to have a negative impact on the spatial resolution. Larger thicknesses of crystal would increase the number of stray photons that undergo multiple reflections before being detected, and also increase the optical light footprint on the PSAPD surface. This would degrade the spatial information of an event [22], the extent of which will be investigated in future experiments.

A small crystal thickness might be a desirable feature for a small-animal imaging system, especially for ^{125}I studies. In this case, a thickness of 0.5 mm of CsI is sufficient to achieve a quantum efficiency near 90%. $LaBr_3$ would stop even more photons, with the additional benefit of producing more light, making it a very attractive crystal for ^{125}I imaging. However, it is still unclear if large sheets of $LaBr_3$ can be manufactured. PSAPDs are particularly well suited for designing a system having a thin scintillator sheet dedicated to ^{125}I imaging, as light spreading over multiple detectors is not required to determine an event position. Such a system would require less material and significantly fewer readout channels than a similar system based, for example, on CZT.

A simple Anger-logic positioning algorithm was implemented in the present work. This linear scheme, when used to read the nonlinear charge division occurring in the resistive layer, creates a distortion in the reconstructed positions, particularly severe near the edges. More complex positioning strategies, for example based on statistics [23], might however be more appropriate, especially for a multiple PSAPDs system. This approach requires a training/calibration phase but on the other hand can probably overcome problems associated with the distortion and with dead space between PSAPDs in the tiled pattern.

V. Conclusion

The present work demonstrates the possibility of using a continuous crystal with a PSAPD to achieve high spatial resolution. Experimental results, corroborated by simulations, showed that submillimeter spatial resolution is possible with this configuration. However, three limiting factors must be considered regarding the results presented here: the thin crystal used, the operation of the PSAPD at low temperatures (-60 °C) and the small detection area. Future work will evaluate the performance with thicker crystals and will explore solutions to expand the detection area, for example by tiling multiple PSAPDs under a single continuous crystal. PSAPDs can be made with a deadspace of $\approx$100 μm along their edges. However, this physical deadspace is expanded by the pincushusion distortion, *i.e.* a $\approx$ 1 mm band along the edges is not useful for imaging, even if segmented crystals are used [8]. A tiled PSAPD approach, combined with a statistical position decoding algorithm, could possibly take care in a transparent way of the pincushion distortion, of the deadspace between PSAPDs and of the positioning problems seen along the edges. The simulation framework developed and validated here will be used to predict the behavior of such a gamma camera. The utilization of thermoelectric coolers (TECs) to achieve low temperatures will also be explored experimentally as an alternative to the liquid nitrogen system used in this work. A continuous crystal, tiled-PSAPD system cooled by TECs would potentially be very attractive for small-animal ^{125}I imaging in terms of cost, simplicity and performance. Dedicated organ imaging in humans is also a potential application, especially if thicker crystals can be used without affecting too much the spatial resolution.

Acknowledgments

This work was supported by NIH grant 2R44 HL078295-02.

References

[1] K. S. Shah, R. Farrell, R. Grazioso, E. S. Harmon, and E. Karplus, "Position-sensitive avalanche photodiodes for gamma-ray imaging," *IEEE Trans. Nucl. Sci.*, vol. 49, no. 4, pp. 1687–1692, 2002.

[2] W. Barber, T. Funk, M. McClish, K. Shah, and B. Hasegawa, "PSAPD gamma camera for SPECT imaging," in *Nuclear Science Symposium Conference Record, 2004 IEEE*, vol. 5, 2004, pp. 2815–2817.

[3] C. Levin, A. Foudray, P. Olcott, and F. Habte, "Investigation of position sensitive avalanche photodiodes for a new high-resolution PET detector design," *IEEE Trans. Nucl. Sci.*, vol. 51, no. 3, pp. 805–810, 2004.

[4] K. Shah, R. Grazioso, R. Farrell, J. Glodo, M. McClish, G. Entine, P. Dokhale, and S. Cherry, "Position sensitive APDs for small animal PET imaging," *IEEE Trans. Nucl. Sci.*, vol. 51, no. 1, pp. 91–5, 2004.

[5] K. C. Burr, A. Ivan, J. LeBlanc, S. Zelakiewicz, D. L. McDaniel, C. L. Kim, A. Ganin, K. S. Shah, R. Grazioso, R. Farrell, and J. Glodo, "Evaluation of a position sensitive avalanche photodiode for PET," *IEEE Trans. Nucl. Sci.*, vol. 50, no. 4, pp. 792–796, 2003.

[6] D. Paix, "Pinhole imaging of gamma rays," *Phys. Med. Biol.*, vol. 12, no. 4, pp. 489–500, 1967.

[7] M. Moszynski, M. Szawlowski, M. Kapusta, and M. Balcerzyk, "Large area avalanche photodiodes in scintillation and X-rays detection," *Nucl. Instr. and Meth. A*, vol. 485, no. 3, pp. 504–521, 2002.

[8] P. Després, W. C. Barber, T. Funk, M. McClish, K. S. Shah, and B. H. Hasegawa, "Modeling and correction of spatial distortion in position-sensitive avalanche photodiodes," *IEEE Trans. Nucl. Sci.*, 2006, (submitted, TNS-00061-2006).

[9] V. N. Solovov, F. Neves, V. Chepel, M. I. Lopes, R. F. Marques, and A. J. P. L. Policarpo, "Low-temperature performance of a large area avalanche photodiode," *Nucl. Instr. and Meth. A*, vol. 504, pp. 53–57, 2003.

[10] L. M. P. Fernandes, J. A. M. Lopes, and J. M. F. dos Santos, "Excess noise factor in large area avalanche photodiodes for different temperatures," *Nucl. Instr. and Meth. A*, vol. 531, no. 3, pp. 566–568, 2004.

[11] L. Ludhova, F. Amaro, A. Antognini, F. Biraben, J. Cardoso, C. Conde, D. Covita, A. Dax, S. Dhawan, and L. Fernandes, "Planar LAAPDs: temperature dependence, performance, and application in low-energy X-ray spectroscopy," *Nucl. Instr. and Meth. A*, vol. 540, no. 1, pp. 169–179, 2005.

[12] S. Jan *et al.*, "GATE: a simulation toolkit for PET and SPECT," *Phys. Med. Biol.*, vol. 49, no. 19, pp. 4543–4561, 2004.

[13] S. Agostinelli *et al.*, "GEANT4 – a simulation toolkit," *Nucl. Instr. and Meth. in Phys. Res. A*, vol. 506, pp. 250–303, 2003.

[14] G. Knoll, T. Knoll, and T. Henderson, "Light collection in scintillation detector composites for neutron detection," *IEEE Trans. Nucl. Sci.*, vol. 35, no. 1, pp. 872–875, 1988.

[15] A. Levin and C. Moisan, "A more physical approach to model the surface treatment of scintillation counters and its implementation into DETECT," in *Nuclear Science Symposium Conference Record, 1996 IEEE*, vol. 2, 1996, pp. 702–706.

[16] S. Nayar, K. Ikeuchi, and T. Kanade, "Surface reflection: physical and geometrical perspectives," *IEEE Transactions on Pattern Analysis and Machine Intelligence*, vol. 13, no. 7, pp. 611–634, 1991.

[17] M. McClish, Radiation Monitoring Devices Inc., private communication.

[18] J. E. Eldridge, *Handbook of Optical Constants of Solids II*. Academic Press, 1991, ch. Cesium Iodide (CsI), pp. 853–874.

[19] F.-X. Gentit, "Litrani: a general purpose monte-carlo program simulating light propagation in isotropic or anisotropic media," *Nucl. Instr. and Meth. A*, vol. 486, no. 1-2, pp. 35–39, 2002.

[20] R. Brun and F. Rademakers, "ROOT - an object oriented data analysis framework," *Nucl. Instr. and Meth. in Phys. Res. A*, vol. 389, pp. 81–86, 1997.

[21] M. J. Berger, J. H. Hubbell, S. M. Seltzer, J. S. Coursey, and D. S. Zucker, "XCOM: Photon cross section database (version 1.2)," National Institute of Standards and Technology, Gaithersburg MD, Tech. Rep., 1999, originally published as NBSIR 87-3597, National Institute of Standards and Technology, Gaithersburg, MD (1987). [Online]. Available: http://physics.nist.gov/xcom

[22] F. A. Harrison, S. M. Kahn, C. J. Hailey, and K. Ziock, "Performance optimization for hard x-ray/soft gamma-ray detectors," in *Proceedings of SPIE*, vol. 1344, no. 1. San Diego, CA, USA: SPIE, Nov. 1990, pp. 47–52.

[23] J. Joung, R. S. Miyaoka, and T. K. Lewellen, "cMiCE: a high resolution animal PET using continuous LSO with a statistics based positioning scheme," *Nucl. Instr. and Meth. A*, vol. 489, no. 1-3, pp. 584–598, 2002.